Received: 23 May 2023 | Revised: 14 September 2023 | Accepted: 25 September 2023

DOI: 10.1002/hbm.26511

RESEARCH ARTICLE

WILEY

Integration and segregation manifolds in the brain ensure cognitive flexibility during tasks and rest

Katerina Capouskova[1] | Gorka Zamora-López[1] | Morten L. Kringelbach[2,3,4] | Gustavo Deco[1,5]

[1]Center for Brain and Cognition, Computational Neuroscience Group, DTIC, Universitat Pompeu Fabra, Barcelona, Spain

[2]Department of Psychiatry, University of Oxford, Oxford, United Kingdom

[3]Center for Music in the Brain, Department of Clinical Medicine, Aarhus University, Aarhus, Denmark

[4]Centre for Eudaimonia and Human Flourishing, Linacre College, University of Oxford, Oxford, United Kingdom

[5]Institució Catalana de Recerca i Estudis Avançats (ICREA), Barcelona, Spain

Correspondence
Katerina Capouskova, Center for Brain and Cognition, Computational Neuroscience Group, DTIC, Universitat Pompeu Fabra, Ramon Trias Fargas 25-27, 08005 Barcelona, Spain.
Email: katerina.capouskova@upf.edu

Funding information
Human Brain Project, Grant/Award Number: 945539; EU H2020 FET Flagship Programme; ERC Consolidator Grant: CAREGIVING, Grant/Award Number: 615539; Danish National Research Foundation, Grant/Award Number: DNRF117; Pettit and Carlsberg Foundations; Project PID2022-136216NB-I00 financed by the MCIN /AEI /10.13039/501100011033 / FEDER, UE., the Ministry of Science and Innovation, the State Research Agency and the European Regional Development Fund, Grant/Award Number: PID2022-136216NB-I00; AGAUR research support grant (ref. 2021 SGR 00917) funded by the Department of Research and Universities of the Generalitat of Catalunya, Grant/Award Number: 2021SGR00917

Abstract

Adapting to a constantly changing environment requires the human brain to flexibly switch among many demanding cognitive tasks, processing both specialized and integrated information associated with the activity in functional networks over time. In this study, we investigated the nature of the temporal alternation between segregated and integrated states in the brain during rest and six cognitive tasks using functional MRI. We employed a deep autoencoder to explore the 2D latent space associated with the segregated and integrated states. Our results show that the integrated state occupies less space in the latent space manifold compared to the segregated states. Moreover, the integrated state is characterized by lower entropy of occupancy than the segregated state, suggesting that integration plays a consolidating role, while segregation may serve as cognitive expertness. Comparing rest and the tasks, we found that rest exhibits higher entropy of occupancy, indicating a more random wandering of the mind compared to the expected focus during task performance. Our study demonstrates that both transient, short-lived integrated and segregated states are present during rest and task performance, flexibly switching between them, with integration serving as information compression and segregation related to information specialization.

KEYWORDS
brain states, fMRI, HCP data set, integration, latent space, manifold, segregation

1 | INTRODUCTION

Confronted with the multimodality of the environment the brain must flexibly and swiftly respond. Therefore, it processes the information from the different modalities and yet also provides coherent global behaviour and comprehension. How the brain orchestrates this has been the topic of several theories and is nowadays commonly phrased as the ability of the brain to simultaneously segregate and integrate information (Baars, 2009; Bressler & Kelso, 2001; Damasio, 1989; Dehaene & Changeux, 2011; Tononi, 2004). From an anatomical point of view, it has been shown in the recent decades that the long-range white matter connectivity of the mammalian brain is modular (Hilgetag & Kaiser, 2004; Scannell et al., 1995; Scannell & Young, 1993) and that the cross-modular connections are centralised through hub regions (van den Heuvel & Sporns, 2011; Zamora-López et al., 2010). This modular and hierarchical organization supported the hypothesis that the modular organization is fundamental to facilitate the specialised, segregated processing, while the hubs could assist in integrating multisensory information (Shanahan et al., 2013; Zamora-López et al., 2011).

Evidence from brain activity during rest and tasks has very much confirmed these ideas. The brain, whose architecture is practically unaltered in the time-scales of its activity, effectively engages in multiple tasks by the activation of networks that give rise to different functionality. On the one hand, neuroimaging data have shown that semi-specialised networks activate during specific tasks, triggering the activation of hubs regions when integration is required (Cocuzza et al., 2020; Senden et al., 2017; Senden et al., 2018). On the other hand, brain activity rapidly switches from one functional network to another under task demands (Deco et al., 2015; Power et al., 2011; Ren et al., 2017) including the switching from segregated and integrated states (Cole et al., 2013; Mohr et al., 2016; Wang et al., 2021) that also happen on different temporal scales (Bassett et al., 2011). Even at rest—when no task is demanded—the brain activity is known to perpetually wander, switching between short-living, temporary states (Betzel et al., 2016) rooted in a manifold of metastable states (Rué-Queralt et al., 2021).

The manifold can be thought of as a representation of the brain's underlying structure and organization, and provides a way to analyse and understand the complex patterns of neural activity that give rise to perception, thought, and behaviour (Gao et al., 2021; Gao & Ganguli, 2015; Rué-Queralt et al., 2021; Shine et al., 2019). Various techniques, such as manifold learning and dimensionality reduction, can be used to uncover these neural manifolds and gain insights into brain function (Casanova et al., 2021; Kumar et al., 2018; McInnes et al., 2018). The advantage of representing neural data on an underlying manifold is not only its easier interpretability, but also revealing relationships and structures without the unnecessary noise that is carried in the multidimensional signal (Altan et al., 2021; Plassard et al., 2018). Previous studies observed that the low-dimensional intrinsic manifold is manifested in both tasks (Chaudhuri et al., 2019; Gallego et al., 2017; Williams et al., 2018) and rest (Chaudhuri et al., 2019; Rué-Queralt et al., 2021), which is known for its rich dynamical excitations (Demirtaş et al., 2019; Escrichs et al., 2019; Vohryzek et al., 2020). However, the characteristics of a low-dimensional representation of integrated and segregated brain states in rest and task conditions remain unrevealed together with its implications for the states' functions on the whole-brain level. In this article, we tackle the problem how can we reveal the 2D manifold of integration and segregation states and what the manifold can tell us about the two modes of operation.

In order to solve this problem, in this study we examined the underlying manifolds behind brain activity leading to integration or segregation in the human brain while performing six cognitive tasks and at rest from the Human Connectome Project (HCP) fMRI dataset, where we selected 100 healthy adults. We employed an autoencoder to access a 2D manifold of dynamically changing functional connectivity during the scanning sessions. First, the functional connectivity matrices are clustered according to their modularity and global efficiency measures, and then their compression level is reached after encoding layers in the autoencoder. The first half of the autoencoder consists of layers that compress the signal while reducing noise and keeping the informative parts. After the encoding layers, the latent space representation tells us how similar data points are while they are compressed. The more similar they are, the less latent space they occupy and the easier it is to predict where new data points would be. A compression of the signal should allow the brain to gain flexibility in information exchange and subsequent segregation as it requires less storage space and uses less energy to be transferred. Compression, in the form of encoding, for example, in artificial neural networks, also filters out noise and preserves only important features (Zhuang et al., 2017), which may give rise to the unity of our experience and the necessary adaptability in diverse cognitive activities (He et al., 2019). Hence, we defined integration as a state when information flows from many nodes to one. We hypothesised that integration is a state with compressed information and as such, is represented in the latent space with fewer dimensions. On the other hand, we hypothesize that segregation is a projection of information to specialised subnetworks on a complex manifold, and here the relationship can be the one-to-many projection of an information flow or a one-to-one projection.

In summary, we expect that the integration state to be associated with lower entropy compared with the segregated state and that in the segregated state, classification of different task modalities or resting-state would be more accurate compared with the integrated state because of specialisation in segregation. In our analyses, the processes of integration and segregation are presented in a timeframe which we call a state (Cabral et al., 2017; Capouskova et al., 2022; Vila-Vidal et al., 2019). By characterizing the integrated and segregated states and their dynamical manifolds, we can better understand how brain achieves both cognitive flexibility as an ability to learn many different tasks and specialization as a good proficiency in the tasks (Ito & Murray, 2021; Yang et al., 2019).

2 | MATERIALS AND METHODS

To assess the hypotheses, we used a computational fMRI data analysis with application of a neural network to achieve non-linear lower

dimensions that are accessed not only in space [like principal component analysis (PCA) or leading eigenvector] but also in time. We applied phase coherence on pre-processed fMRI data which have been converted into phases with Hilbert transform to obtain a dFC matrix ($n \times n \times t$, where n stands for the number of brain areas, and t is the number of recorded time points) for each time point (Figure 1a). To cluster for segregated and integrated states, we used modularity and global efficiency as measure representatives of integration and segregation in networks, inspired by Cohen and D'Esposito (2016) (Figure 1b), followed by an autoencoder to get a latent space representation of the two states (Figure 1d). From the 2D latent space, we calculated entropy of the two states (Figure 1f), and finally, we included a classification in the states (Figure 1g).

2.1 | Ethics

All participants gave their full informed consent prior to the study, following the Washington University–University of Minnesota (WU-Minn HCP) Consortium research manual and ethical guidelines. In addition, the study was accredited by the Washington University review board.

2.2 | Participants

For this study, a representative dataset of 1003 participants was picked from the March 2017 public data release from the HCP. The

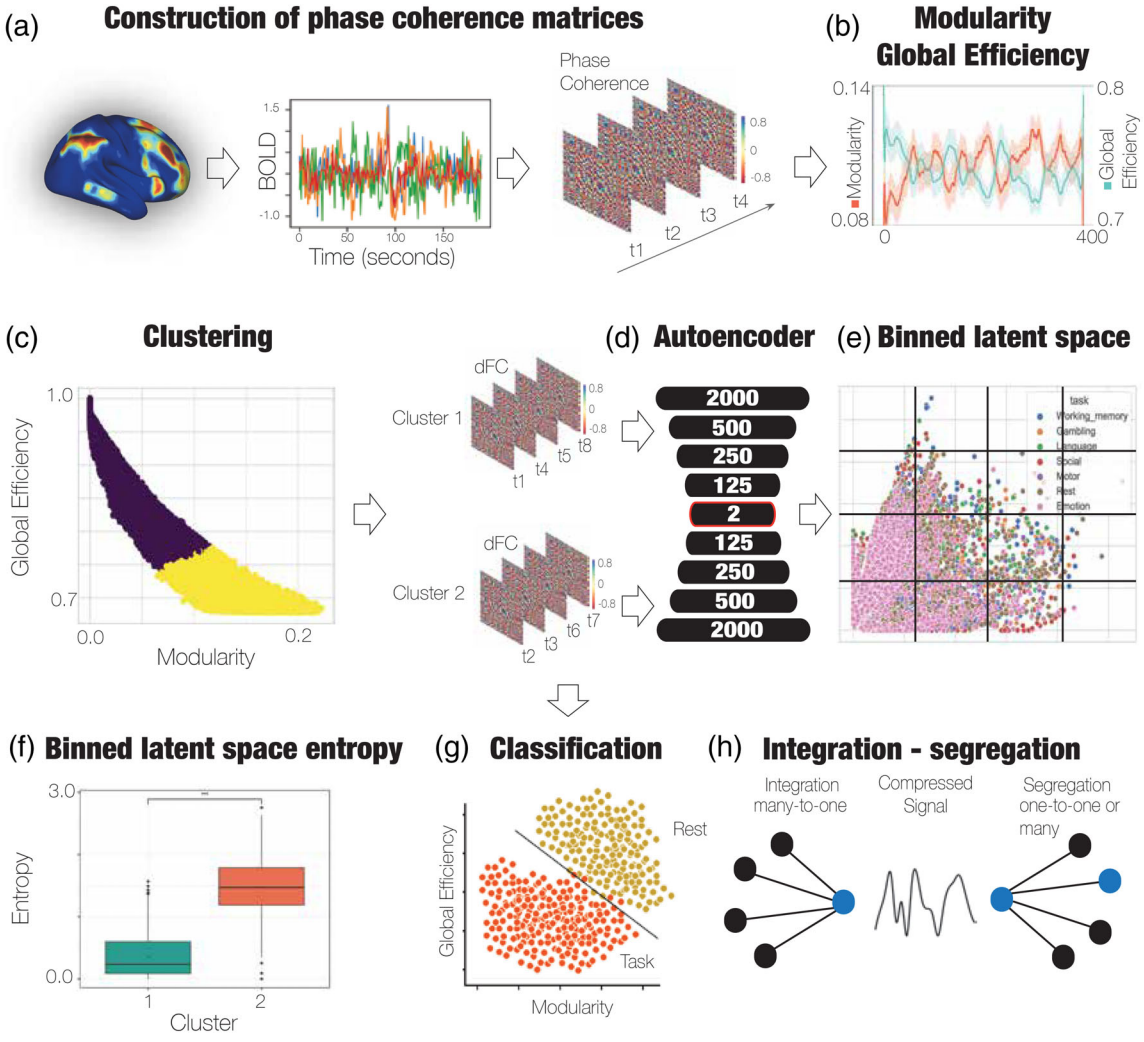

FIGURE 1 General integration-segregation detection analysis representation. (a) BOLD signals from one subject at various brain areas ($N = 80$). BOLD signals are further filtered with a second-order Butterworth filter and converted into phases of a BOLD signal via the Hilbert transform, and with BOLD phase coherence connectivity, dynamic functional connectivity (dFC) is computed. At each time point t, the cosine function of the BOLD phase difference between brain area b1 and brain area b2 yields a symmetric NxN dFC (b1, b2, t) matrix. (b) Estimation of modularity and global efficiency for each dFC for each subject and modality. (c) K-means clustering model dividing dFCs into two states according to modularity and global efficiency. Division of dFCs is according to the cluster belonging for each time point. (d) Deep autoencoder with 10 layers (9 hidden and 1 output layer). (e) 2D latent space as encoded in the autoencoder and binned into a predefined number of bins. (f) Entropy calculated from probability of being in a certain bin of the latent space. (g) Classification of tasks and rest in the two states as defined by clustering. (h) General schema of integration and segregation.

subsequent choice of a down-sampled dataset selected 100 unrelated participants (54 females, 46 males, mean age = 29.1 ± 3.7 years). The second selection ensures the participants are not related, an important benchmark for omitting potential detected confounds. This also excludes the necessity of accounting for family-structure co-variables in the study.

2.3 | Neuroimaging acquisition for fMRI HCP

A Siemens 3-T connecome-Skyra scanner was used to scan all the 1003 HCP participants. In two planned scanning sessions, one session was comprised of working memory, gambling, and motor tasks. The second session included language, social cognition, relational-processing, and emotion-processing tasks. In one session, participants were scanned during rest while looking at a projected bright cross on a dark background for approximately 15 min. The full dataset with all specifics about the subjects, the scanning protocol, and detailed pre-processing of the data for all cognitive tasks and rest sessions can be viewed at the HCP website (http://www.humanconnectome.org/).

2.4 | HCP tasks

For the purpose of the HCP study data, seven cognitive tasks were chosen: working memory, motor, gambling, language, social, emotional, and relational, which are explained in greater detail on the HCP website (Barch et al., 2013). The tasks were selected to activate particular brain regions associated with distinct cognitive and affective processes. The activations were selected across neural systems like cortical and subcortical and with high sensitivity across subjects. We filtered the six most distinct tasks from the set of HCP tasks. There is a shape identification present in the relational-processing task, which is similarly tested in the emotion-processing task.

2.5 | Parcellations

For parcellations, commonly used atlases were utilised to prepare all neuroimaging data with the addition of subcortical regions. To achieve a less refined parcellation, the Mindboggle-modified Desikan–Killiany (DK) parcellation (Desikan et al., 2006) was adopted (in comparison with the Glasser parcellation (Glasser et al., 2016), because extra dimensionality reductions were processed in the study). The final DK parcellation comprised a total of 62 cortical regions, 31 regions per hemisphere (Klein & Tourville, 2012). We also added 18 subcortical regions, nine regions per hemisphere: hippocampus, amygdala, subthalamic nucleus, globus pallidus internal segment, globus pallidus external segment, putamen, caudate, nucleus accumbens, and thalamus. With the added subcortical regions, a final parcellation was achieved consisting of 80 regions in the DBS80 parcellation, with a precise demarcation in the common HCP CIFTI 'grayordinates' standard space.

2.6 | Pre-processing and extraction of functional time series in fMRI resting state and task data

A comprehensive explanation of the pre-processing of the HCP resting state and task datasets can be viewed on the HCP website (https://github.com/Washington-University/HCPpipelines/wiki/Installation-and-Usage-Instructions). To concisely outline, the HCP pre-processing pipeline was utilised for both the rest and task data, which apply standardised methods adopting the FMRIB Software Library (FSL), FreeSurfer, and the Connectome Workbench software (Glasser et al., 2013; Smith et al., 2013). The pre-processing pipeline included a correction for spatial and gradient deformities and head motion, intensity normalisation and bias field removal, registration to the T1 weighted structural image, transformation to the 2 mm Montreal Neurological Institute space, and, in rest, the use of the FIX artefact removal procedure (Navarro Schröder et al., 2015; Smith et al., 2013). In addition, in rest data in the pre-processing procedure, head motion noise was regressed out, and structured artefacts were removed by ICA analysis denoising and the FIX method [independent component analysis followed by FMRIB's ICA-based X-noisifier (Griffanti et al., 2014; Salimi-Khorshidi et al., 2014)]. Further details about the ICA-FIX method can be accessed via https://github.com/Washington-University/HCPpipelines/blob/master/ICAFIX/README.md. The refined time series of all 'grayordinates' are placed in HCP CIFTI 'grayordinates' standard space and are accessible in the surface-based CIFTI file for each participant for the resting state and each task. A custom-built Matlab script was programmed for utilising the ft_read_cifti function from the Fieldtrip toolbox (Oostenveld et al., 2011) to obtain the average time series of all the 'grayordinates' in each brain area of the Glasser and DBS80 parcellations, which are defined in the HCP CIFTI 'grayordinates' standard space. The pre-processing protocol included a second-order Butterworth filter in the span of 0.008–0.08 Hz to smooth the BOLD signal from both task and rest data. For all the task and rest data, we first selected only 175 time points (corresponding to the lowest number of time points in the dataset—here, the emotion task) to have balanced data for further analyses.

2.7 | Dynamic functional connectivity

To account for the underlying time dynamics, we employed a time-sensitive dFC matrix. For its construction, the BOLD phase coherence connectivity was used (Deco et al., 2017; Deco & Kringelbach, 2016; Ponce-Alvarez et al., 2015). The resulting dFC has $n \times n \times t$ dimensions, where n is the number of brain areas—80 in the applied DBS80 parcellation—and t is the total number of all time points in the neuroimaging recordings for each task and rest. First, we used a second-order Butterworth filter to smooth the BOLD signal. We estimated the phases of the filtered BOLD signals via the Hilbert transform in all brain areas n, getting a phase coherence estimation $\theta(n, t)$. The dFC is computed as a cosine similarity amongst phases of brain areas n and p at time t: $dFC(n, p, t)$ as follows:

$$d(n,p,t) = \cos(\theta(n,t) - \theta(p,t)),$$

where cos() is the cosine function. The cosine function proved to be beneficial for data scaling as with cos(0) = 1 for areas which occupy a homologous phase for a moment, their BOLD signals are harmonious, and their dFC(*n*, *p*, *t*) is approximately 1. In the case, when two BOLD signals are not consistent with each other, and they are orthogonal, the dFC(*n*, *p*, *t*) is around 0. In the phase coherence estimation, the computation only assigns distances without direction between two phases; hence, the subsequent matrix is undirected. With the characteristic of undirectedness, the matrix is symmetric, and all the relevant information can be obtained from the upper or lower triangular part of the matrix.

2.8 | Modularity and global efficiency

Modularity is a measure that evaluates the goodness of a partition of network into modules (Newman, 2004), that is, how well the network is split into groups. Therefore, it is very popular as the cost function for community detection algorithms in networks, which aim at maximising modularity. Modularity is defined as follows:

$$Q = \frac{1}{2m}\sum_{ij}\left(A_{ij} - \frac{k_i k_j}{2m}\right)\delta(c_i, c_j);$$

where m stands for the number of edges, A_{ij} is the adjacency matrix, k_i is the degree of i, and δ is 1 if i and j belong to the same community; otherwise, it is 0. In this study, we used the Louvain algorithm (Blondel et al., 2008) for community detection in a weighted und undirected graph (Reichardt & Bornholdt, 2006). We calculated modularity to assess the prevalence of connections inside communities compared with connections between communities.

To quantify the distance between nodes we employed the weighted global efficiency measure (Latora & Marchiori, 2001; Latora & Marchiori, 2003), which is robust for the case of disconnected nodes when networks are sparse. Global efficiency G is estimated as the average of the pair-wise efficiency (inverse of the shortest path) between the nodes of a network:

$$E(G) = \frac{1}{n(n-1)}\sum_{i \neq j}\frac{1}{d_{ij}},$$

where d_{ij} is a weighted shortest-path distance between nodes i and j (the minimum sum of weights across all the paths connecting i and j), and n is the number of nodes.

2.9 | Integrated and segregated states—K-means clustering

After estimating modularity and global efficiency for each time point, subject, and condition, we applied an unsupervised machine-learning method to identify the two states: integrated and segregated. There is also an option to select three (or more) states, where one state would serve as a transitional; however, for a good comparison between segregated and integrated, we opted for only two fixed states. We used the k-means clustering method implementation in scikit-learn in Python (Pedregosa et al., 2011) to cluster for the two states. For quality and validity of the clustering separation evaluation, we applied the silhouette score (Rousseeuw, 1987; Figure 3a). For tolerably separated clusters, the average silhouette coefficient should be at least 0.51 (Kaufman & Rousseeuw, 2005).

2.10 | Autoencoder

To compare how the integrated and segregated states are represented in space, we had to include a dimensionality reduction method as the dFC matrix of $n \times n$ dimensions is too complex to compare with a high number of insignificant features (Ronan et al., 2016). Although traditional methods such as PCA are easy to implement, their linear characteristics would not reveal the underlying manifold of the data in such scope. For the data representation (the dFCs) in a lower-dimensional space, we implemented a nonlinear data transformation 10-layer-deep autoencoder algorithm. In our case, the latent space is represented only in two features to get a 2D space which is easy to visualise and analyse; however, other dimensions might capture the dynamics more appropriately. We ran one autoencoder for both states at the same time. We also checked if training a balanced dataset [by using oversampling from imbalanced-learn (Lemaître et al., 2017)] for both integrated and segregated data produces different results; however, the distinction between the latent space representation in both is still evident (Figure 1 in Supplementary materials). Thus, we opted to use the latent space of an autoencoder trained on unbalanced (real) data points to obtain task and rest differences in the further analyses.

An autoencoder is a special case of an artificial neural network, which is set with random weights trained all at once by minimising the discrepancy between the original data and their reconstruction. An autoencoder is composed of three elements: the encoder, the code, and the decoder. In the first encoder component, the model learns through training to compress the data into an encoded representation. Code is the encoded compressed data representation in a latent space. Finally, in the decoder, the model is trained to reproduce the input data from the latent space. The reconstruction is optimised to be as close to the original data as possible. The most common training technique is backpropagation, where error derivatives are propagated through the decoder and encoder parts to optimise the weights in the network. The encoder input space ($\mathcal{X}$) and decoder input space ($\mathcal{F}$) are defined as transitions (ϕ,ψ) which minimise the reconstruction loss so that the divergence between the input data and the output data are reduced and can be defined as follows:

$$\phi : \mathcal{X} \to \mathcal{F}$$

$$\psi : \mathcal{F} \to \mathcal{X}$$

$$\phi,\psi = \underset{\phi,\psi}{\operatorname{argmin}} \| X - (\psi^{\circ}\phi)X\|^2$$

The autoencoder we employed was structured as a 2000-500-250-125-2-125-250-500-2000 schema, inspired by Hinton and Salakhutdinov (2006), with the middle layer of latent space serving as the output layer for our further analysis with the encoded vector $E(t)$. The input dataset to our autoencoder was a dataset consisting of dFCs for each time point, each task or rest modalities and each subject. For the autoencoder, each data point was represented by one dFC. We used gradient-based Adam (adaptive movement estimation) learning rate optimisation that automatically adapts a learning rate for each input variable for the objective function and is now considered a state-of-the-art technique (Kingma & Ba, 2014). We applied a mean squared error loss function that measures the average squared difference between the predicted values and the actual target values to check for the goodness of the encoding. In the activation function, and the autoencoder ran on a rectified linear unit (ReLu) function that outputs positive input directly and negative input as zero (Agarap, 2018) with 30 epochs (number of iterations of training the whole set of training data; estimated from previous runs as optimal) and a batch size of 100 (number of samples processed before updating the model). We run the autoencoder with different parameters like different activation functions (combination of ReLu and linear, and sigmoid function), cross-entropy loss function and different batch sizes, which all produced similar results to the final autoencoder.

2.11 | Binned latent space and entropy

With a latent space of two features, we constructed a 2D space for both integrated and segregated states which we binned (divided space into subsections; Figure 3E) by implementing a function binned_statistics_2D in SciPy (Virtanen et al., 2020). Within the individual bins, we counted the number of present data points for each condition, subject, and cluster (integrated or segregated). We created a list with each bin's number of points divided by all the points in the space (also for each subject, condition, and cluster) to count for a data point's probability of being in the specific bin.

After having a list of probabilities of occurrences in the bins for each condition, subject, and cluster, we calculated the entropy of the occurrence. Shannon entropy is estimated using the following equation:

$$H(X) = -\sum p(x) \log p(x);$$

where $p(x)$ is the probability of being in a bin. From the entropy, we obtained an estimate of compression of data in the latent space. As the data become more compressed, the occupancy in the latent space decreases ($p(x)$ approaches a distribution in which only one bin is occupied), leading to a decrease in entropy. If the data are hard to compress, the occupancy in the latent space tends to become uniform ($p(x)$ approaches a distribution in which all bins are equally occupied), resulting in a high entropy.

2.12 | Classification

We fitted two multiclass support vector machine (SVM) classification algorithms to determine the divisibility of each task and rest based on 80 features (individual measurable properties) taken from the leading eigenvector of each dFC. The two classification models were trained on data clustered as either integrated or segregated. We preferred SVM as it showed a higher performance compared to the k-neighbour and logistic regression in terms of accuracy and overfitting. Furthermore, we utilised a grid search algorithm to search for the optimal parameters and used k-fold cross-validation with five folds to estimate the performance of training and testing on the subset data for the split of 20% test data and 80% training data. We balanced the number of data points for each class according to the lowest occurring number of points: 3282.

2.13 | Between-conditions comparisons

We used a permutation-based paired t test to discover significant differences between groups. This is a nonparametric two-sample hypothesis test which employs permutations of group labels to estimate the null distribution instead of depending on the test-type standard distributions. The null distribution is calculated independently for each condition. We ran the test for each of 5000 permutations to compare populations. All reported p-values were corrected with the Bonferroni method for multiple comparisons.

3 | RESULTS

We closely examined the integration and segregation states in the brain, by showing the probability of being in the states during different cognitive tasks and in rest. We also uncovered the most dominant brain areas in both states. Our main goal was to uncover the occupancy of their latent spaces to show their role in cognition.

3.1 | Modularity and global efficiency

First, we estimated graph metrics for all weighted FC matrices for each condition, subject, and time point. We found a handful of statistical differences between tasks and rest in modularity and global efficiency which pass a permutation-based t test with $p < .01$ Bonferroni corrected (Supplementary Table 1). Figure 2 captures the changing between modularity and global efficiency during the time course of the tasks and rest demonstrating the blocks composition of the tasks and rest. Modularity indicates the structure of a network by its division into communities called modules (Newman, 2004). High modularity means high connectivity inside communities but low connectedness across the whole network (Figure 2c). This feature indicates higher specialisation with high modularity as we presuppose that each module has its own expertise. In this study, high modularity was achieved in rest 0.114

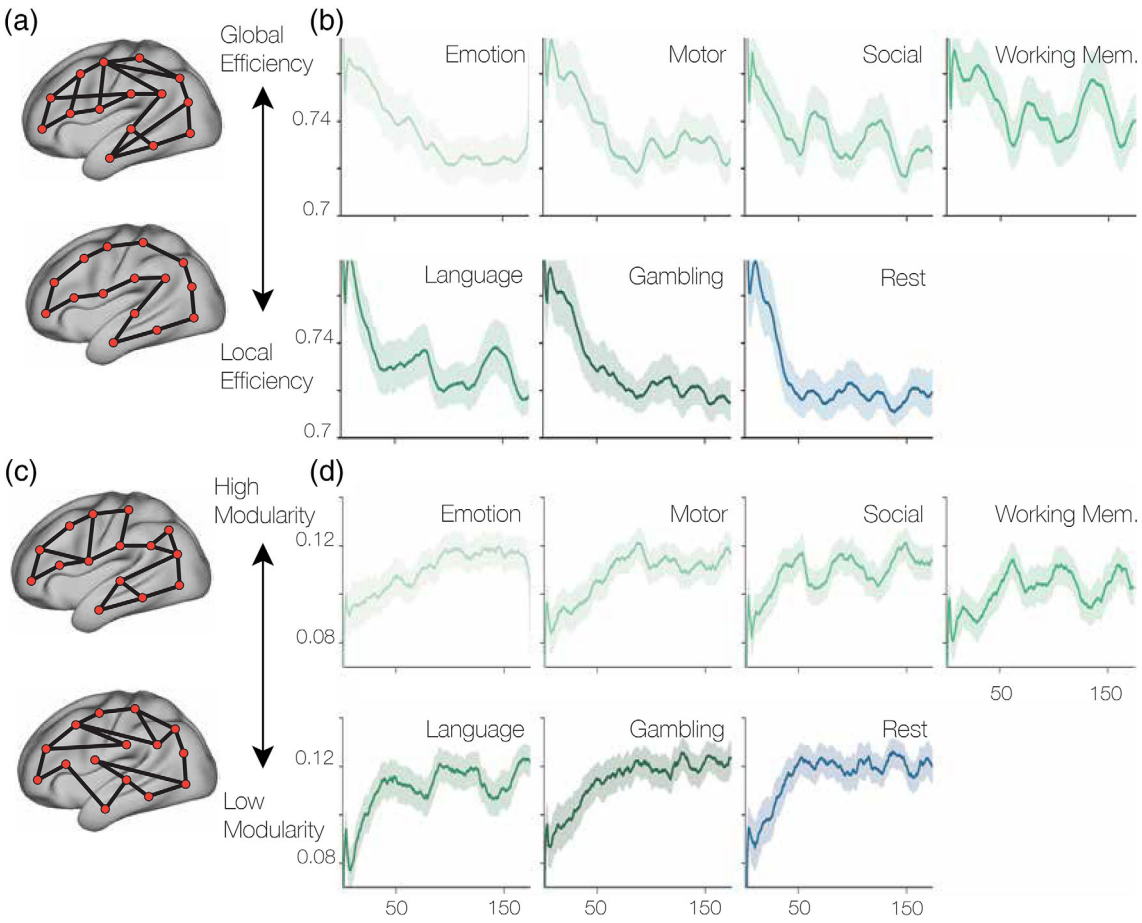

FIGURE 2 Modularity and global efficiency: (a) Illustration of high global efficiency and low global efficiency/local efficiency in a glass brain. (b) Global efficiency as detected in all dFCs by task or rest conditions. Oscillating high and low global efficiency was detected in working memory, social, and language tasks associated with changing of high cognitive load of the tasks. In contrast, low global efficiency was detected in emotion tasks, gambling, and rest. (c) Illustration of high and low modularity in a glass brain. (d) Modularity as measured in all dFCs by task or rest conditions. Similar results were found with global efficiency, oscillating modularity in working memory, social, and language tasks compared with increasing modularity in emotion, motor, gambling, and rest.

± 0.016 (mean ± standard deviation), the gambling task 0.113 ± 0.014, and the emotion task 0.109 ± 0.013, while lower modularity was present in social 0.107 ± 0.013, working memory 0.101 ± 0.101 ± 0.012, and motor tasks 0.107 ± 0.013 (Figure 2d). Higher fluctuations in modularity in the later signal (adjusted after first 50 time points), was in working memory 0.005 (standard deviation), emotion 0.005, social 0.005, and language tasks 0.005 compared with rest 0.003, gambling 0.003, and motor 0.003 tasks.

Global efficiency measures the weighted distance between nodes in a network, in a robust manner against disconnected nodes (Latora & Marchiori, 2001). With high global efficiency, information is indicative of facilitated transfer of information throughout the network. Thus, it is characteristic of high integration between the brain areas (Figure 2a). During the sessions, global efficiency varied, with highest mean level observed during the working memory task 0.748 ± 0.021 (mean ± standard deviation) and emotion 0.738 ± 0.024, social 0.737 ± 0.024 and motor tasks 0.738 ± 0.024. In contrast, global efficiency tended to be lower during rest 0.729 ± 0.029, gambling 0.731 ± 0.025, and language 0.735 ± 0.024 tasks (Figure 2b).

3.2 | Integrated and segregated states

To get the two states defined as integrated and segregated, we used the k-means clustering algorithm on the two features represented by modularity and global efficiency on all subjects ($n = 100$) in all tasks and at rest. This separated all dFCs into two groups. We computed the normalized strength (degree) of connectivity for two mean FC patterns by summing all connections within each brain area (represented by a single row in the dFC matrix) and dividing by the total number of possible connections for that area (i.e., the number of columns in the dFC matrix). The normalised strength indicates how much is a brain region functionally connected with the rest.

In the integrated state (Figure 3d), the region most strongly connected is the left thalamus with the normalised strength of 0.73. Then follow the right superior frontal (0.729), left superior frontal (0.726), right thalamus (0.72), right inferior parietal (0.71), and left inferior parietal (0.71). In the segregated state (Figure 3E), the most connected region is the left thalamus with a normalised strength of 0.37; next is the right superior frontal (0.365), followed by the right thalamus

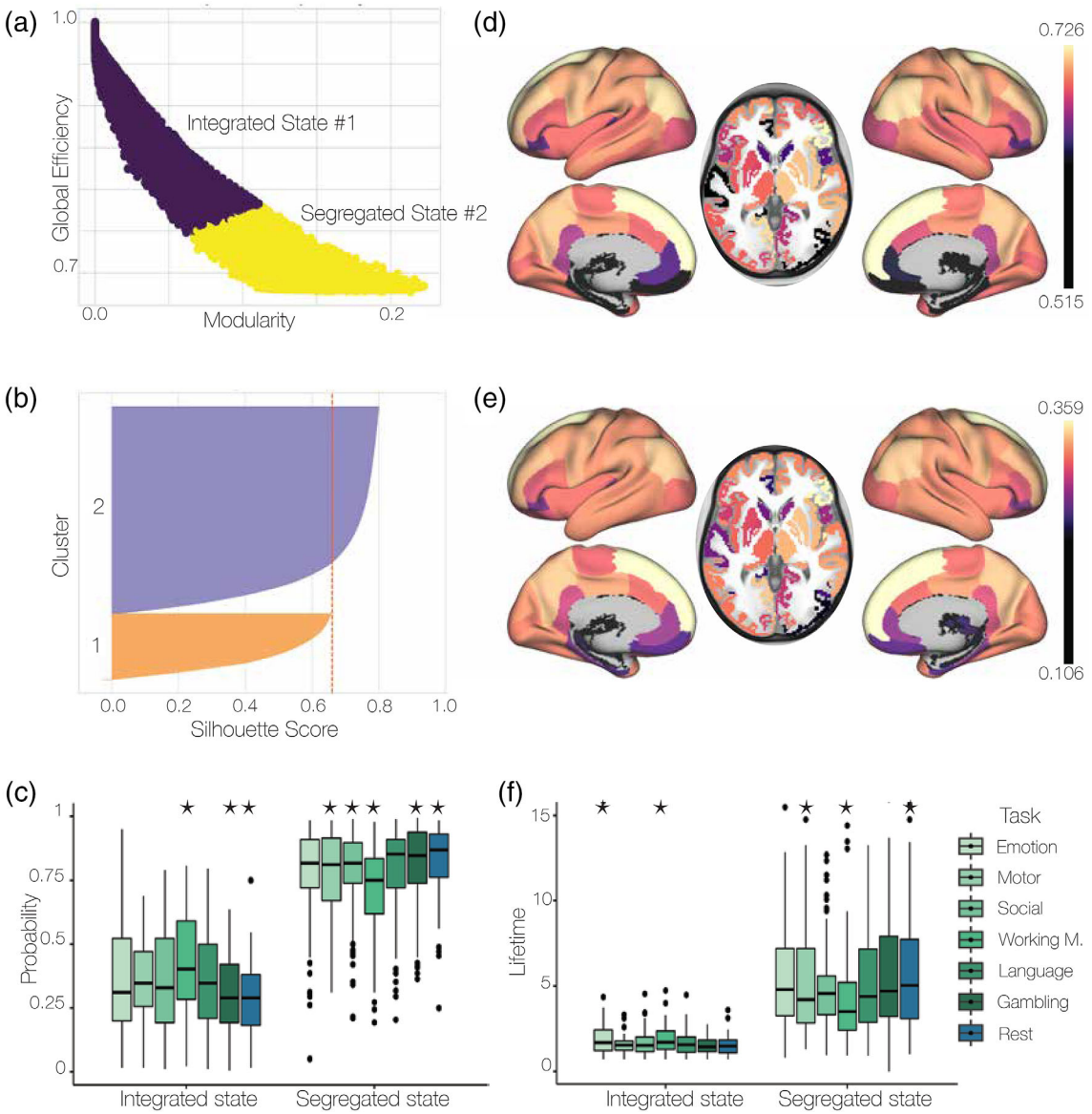

FIGURE 3 Clustering, two brain states, and probability. (a) Clustering of modularity and global efficiency into two states, showing that high global efficiency represents the integrated state, and high modularity is associated with the segregated state. (b) Silhouette score of the k-means clustering, which is above the 0.5 threshold and is accordingly well separated. (c) Probability of occurrence in integrated and segregated states: The highest mean probability of being in an integrated state was found in the working memory task, which was also significantly distinct from all the tasks (permutation-based paired *t* test, $p < 0.01$, Bonferroni correction). The highest mean probability of being in a segregated state was found in rest. Stars indicate a significant difference from all the other conditions [permutation-based paired *t* test ($p < .01$) with Bonferroni correction]. (d) Brain surface and volume renders of the integrated state. The render represents a normalised connectivity strength in the state. Rendered with Connectome Workbench (available at https://www.humanconnectome.org/software/connectome-workbench). (e) Brain surface and volume renders of the segregated state. The render depicts a normalised connectivity strength in the state. (f) Mean lifetimes of integrated and segregated states in all modalities including rest. In an integrated state, the mean lifetimes are relatively short, especially in motor and gambling tasks. In a segregated state, the mean lifetimes are longer, with the emotion task having the longest mean lifetime. Stars indicate a significant difference from all the other conditions [permutation-based paired *t* test ($p < .01$) with Bonferroni correction].

(0.36), left superior frontal (0.359), right inferior parietal (0.33), and left inferior parietal (0.33). In general, the most connected brain areas are the same in both states, including the right and left thalami, right and left superior frontal lobules, and right and left inferior parietal lobules. However, during the integrated states they are connected much stronger to the network than during the segregated states.

We then examined how often and how long are the integrated or the segregated states activate in each of the tasks (language, motor, emotion, social, gambling, and working memory) and rest. For that, we quantified the average probability of each of the two states to happen during an experimental session. Our analysis revealed that segregated states were more likely to occur than integrated states, with a general

higher probability observed across all tasks (Figure 3c). Specifically, the probability of being in a segregated state was highest during rest, with a value of 0.814 ± 0.014 (mean ± standard error of the mean). The gambling task followed with a probability of 0.798 ± 0.015, while the language and emotion tasks had probabilities of 0.766 ± 0.018 and 0.76 ± 0.018, respectively. The social task showed a slightly lower probability of 0.756 ± 0.017, while the motor task was even less probable at 0.744 ± 0.016. The working memory task had the lowest probability of being in a segregated state, with a value of 0.668 ± 0.019.

Conversely, the highest probability of expressing integrated states was in the working memory task 0.332 ± 0.019, emotion task 0.24 ± 0.018, and language task 0.234 ± 0.018. A lower probability of integration was found in the social task 0.244 ± 0.017, motor task 0.256 ± 0.016, and gambling task 0.202 ± 0.015. The least prevalent integration state was revealed in rest, 0.186 ± 0.014.

The longest mean lifetime of a segregated state was measured in the emotion task, 7.255 ± 0.065; followed by the gambling task, 7.155 ± 0.059; and rest, 6.114 ± 0.032. Shorter lifetimes of the segregated state were exhibited in the motor task, 5.726 ± 0.043; emotion task 7.255 ± 0.065; and social task 5.216 ± 0.025. The shortest mean lifetime of the segregated state was identified in the working memory task, 4.401 ± 0.031. In an integrated state, the longest mean lifetime was detected in the emotion task, 2.34 ± 0.044, followed by the working memory task, 1.905 ± 0.01; social task, 1.774 ± 0.013; and language task 1.737 ± 0.013. Relatively shorter mean lifetimes of the integrated state were observed in the motor task, 1.573 ± 0.008; rest, 1.544 ± 0.01; and gambling task 1.542 ± 0.008 (Figure 3f).

The mean silhouette score for the two clusters (0.63) was above the threshold of 0.51 necessary for reasonably separated clusters within the dedicated space (Figure 3b).

3.3 | Autoencoder, binning, and entropy of the latent space

We trained the autoencoder for 30 epochs, as this number was estimated from previous training sessions as optimal for encoding the data into two dimensions with minimal error in the decoder's reconstruction (Figure 4a). We also tested the autoencoder with balanced dataset of integration and segregation datapoints that yielded comparable results (see in Supplementary materials). With 2D latent space, we were able to visualise and analyse the data with the two features, creating a 2D space (Figure 4b,c). Furthermore, we binned the latent space of two features with a different number of bins along each axis. We used 2, 4, 6, 8, 10, 12, 14, 16, 18, and 20 bins along each axis, creating 4, 16, 36, 64, 100, 144, 256, 324, and 400 bins in total. For all those binned latent spaces, we calculated the probability for each subject, condition, and state data point of being in each of the bins. From the probability, we calculated entropy for each of the 10 binned spaces. In each of the 10 binned spaces, entropy of the integrated state was significantly different from entropy of the segregated state with $p < .001$ (more in the supplementary material). We chose the space with 12 bins in each axis to further investigate as it seems to provide balanced space division.

Integrated and segregated states pass a permutation-based t test $(t = -53.177, p = .0004)$ in the 12 bins space scheme. In the same 12-bin separation for both states, we analysed differences amongst all tasks. In the integrated state, only two couples passed a permutation-based t test with $p < .05$ with Bonferroni correction, namely motor and working memory tasks $(t = 4.08, p = .008)$ and working memory task and rest $(t = -3.88, p = .008$; Figure 3D). In the segregated state, task and rest are easier to discriminate from each other. Those which passed permutation-based t tests with Bonferroni correction are the emotion task and rest $(t = -4.12, p = .008)$, motor task and rest $(t = -5.4, p = .008)$, social task and rest $(t = -3.93, p = .008)$, working memory and rest $(t = -53.177, p = .0004)$, and gambling task and rest $(t = -3.77, p = .02$; Figure 3E). We tested for separability inside tasks between the two states for the 12 bins space discretisation. All the tests were permutation-based t tests with Bonferroni correction for multiple comparisons. For the emotion task, the two states are significantly different $(t = -18.04, p = .0004)$, which is similar to the other conditions: motor task $(t = -19.11, p = .0004)$, social task $(t = -21.55, p = .0004)$, working memory task $(t = -22.59, p = .0004)$, language task $(t = -19.95, p = .0004)$, gambling task $(t = -21.32, p = .0004)$, and rest $(t = -21.2, p = .0004$; Figure 3A).

3.4 | Classification

After running several classification methods, we achieved very good separation between rest and the cognitive tasks based on modularity and global efficiency features in the two states. In the integration state, the cross-validated (fivefolds) mean test score was 0.75 in k-nearest neighbours [compared with support vector classifier (SVC), 0.58, and logistic regression, 0.29; Figure 5b]. The cross-validated mean training score was 0.95 in k-nearest neighbours, 0.77 in SVC, and 0.31 in logistic regression. The most correctly predicted label was in the emotion task (0.97). Other tasks had the same score of 0.95 for correctly predicted labels; rest scored 0.95 (Figure 5c). In the segregated state, the separation between tasks and rest based on modularity and global efficiency features scored lower than in the integrated state. The cross-validated mean test score in k-nearest neighbours was 0.525 (0.52 in SVC and 0.24 in logistics regression; Figure 5b). For the training session, the cross-validated mean score was 0.86 in k-nearest neighbours (0.79 in SVC and 0.25 in logistics regression). The most correctly predicted label was in the social task (0.92), followed by emotion and language tasks (0.91). Rest also scored very high in correct label prediction (0.9; Figure 5d).

4 | DISCUSSION

Despite the considerable progress made in understanding the integrated and segregated brain states during rest and task conditions, the characteristics of their low-dimensional representation remain

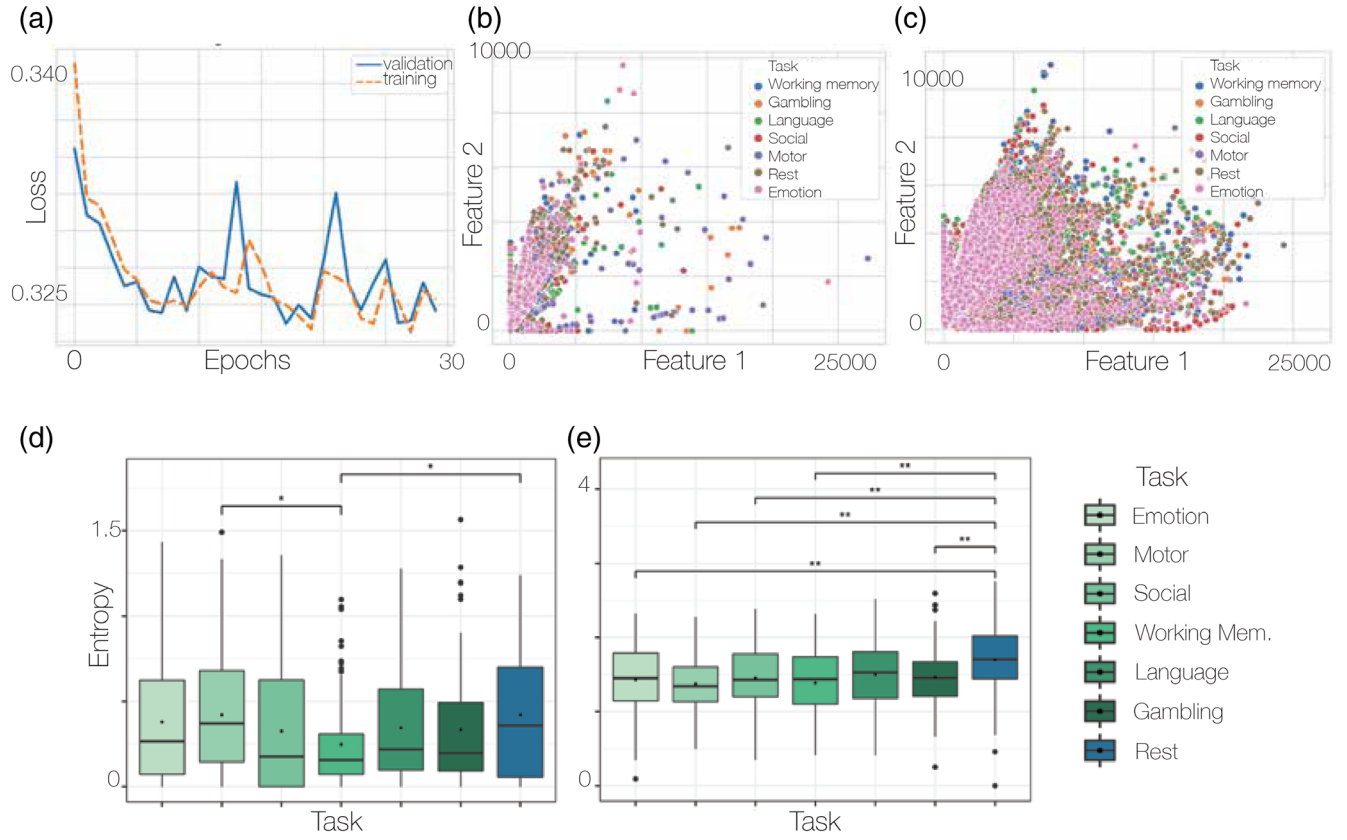

FIGURE 4 Autoencoder and entropy: (a) Loss function for training and validation datasets while the autoencoder was trained for 30 epochs. It should be noted that validation is being calculated after the whole batch is trained; hence, that training starts lower. (b) Latent feature space of the integrated state, which is occupied much less compared with the (c) latent feature space of the segregated state, which is very occupied by data points. (d) Entropy of occupation in the integrated state. The highest mean entropy is in the rest condition, with significant differences to the working memory task. Another significant difference is between the motor task and working memory task (permutation-based paired *t* test, $p < .05$, Bonferroni correction). (e) Entropy of latent space occupation in the segregated state. Rest shows the highest mean entropy, which differs significantly from all the tasks (permutation-based paired *t* test, $p < .005$, Bonferroni correction) except the language task, where $p < .05$ (permutation-based paired *t* test, Bonferroni correction).

unclear, as well as their implications for overall brain function. In this study, we aimed to address this knowledge gap by investigating how we can uncover the 2D manifold of integration and segregation states, and what insights it can provide regarding these two modes of operation. In a 2D latent space, which we were able to reach with an autoencoder, integration's manifold occupies less space compared to segregation, which was measured by lower entropy in integration compared with segregation. This implied that integration, being embedded on a more restricted manifold, serves as a data compression process to not only create a unity of our experience, but also to transfer information more efficiently and flexibly, while segregation serves to benefit cognitive diversity.

After binning the space with different numbers of bins, we chose 12 to analyse further. We calculated entropy of the latent space by estimating the probability for each data point in a particular bin. Highest entropy in both states was in rest. In an integrated state, the difference was significant only from the working memory task; however, in the segregated state, rest entropy was significantly different from all the tasks except language. Higher entropy in rest was previously identified in other studies (Escrichs et al., 2019; Saenger et al., 2018). In rest, brain states are characterised by increased metastability, so the brain's dynamics are less predictable (more random) while visiting a wider dynamical regime. Moreover, in rest, it is harder to predict the state at a particular time point due to higher uncertainty as indicated by a larger entropy (Carhart-Harris et al., 2014). This allows for increased flexibility in learning new tasks with lower precision and specialisation, which is advantageous in settings when no immediate response is necessary—hence, in rest (Fong et al., 2019; Nogueira et al., 2018; Yang et al., 2019). Rest is crucial for generating flexibility in the human brain, providing the foundation for both specialized task performance and the acquisition of new skills.

Inspired by previous studies, we used modularity and global efficiency as indicators of integrated and segregated states (Bouyssi-Kobar et al., 2019; Cohen & D'Esposito, 2016; Keerativittayayut et al., 2018); however, other measures could be used from the family of graph theory or those which reflect the characteristics of integration and segregation of information in the brain. In our case, high global efficiency is associated with an integrated state, that is, a

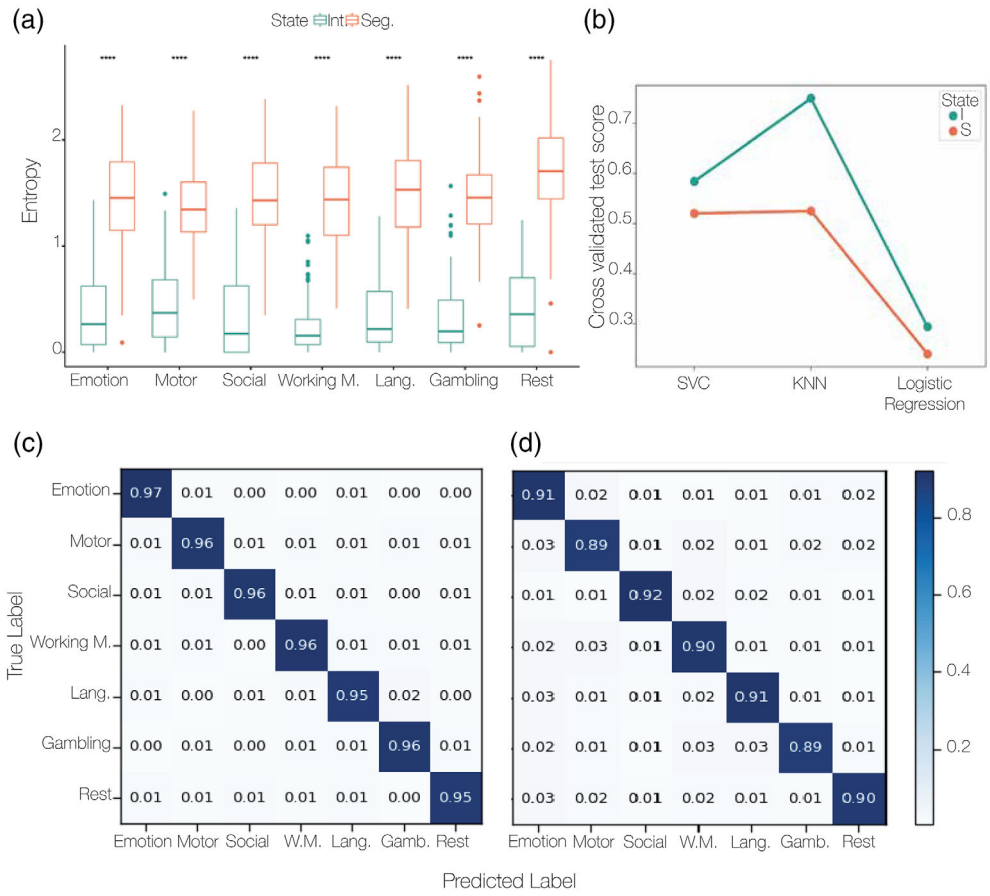

FIGURE 5 Classification: (a) Entropy of latent space occupation in integrated and segregated states for each task. There is a significant difference in all tasks and rest between entropy of latent space occupancy in integrated and segregated states (permutation-based paired *t* test, $p < .0005$, Bonferroni correction). (b) Cross-validated test scores for integrated and segregated states in three different classification models: support vector classifier (SVC), k-nearest neighbour (KNN), and logistic regression. The best score was achieved with KNN, which was above 0.5 in both states, and a better score was achieved in the integrated state. (c) Normalised confusion matrix for integrated state prediction in KNN with good prediction results showing on the diagonal, where the label was predicted properly (score above 0.94). (d) Normalised confusion matrix for segregated state prediction in KNN with good prediction results showing on the diagonal, where the label was predicted correctly (score above 0.88).

stronger interaction amongst the brain areas. On the contrary, segregation defined as high modularity characterises the breakdown of the network into smaller functional and specialised units. We showed that in integration, the enhanced connectivity between distant areas is supported by compressing information and resulting in lower entropy. This is due to the main involvement of structural hubs in the human brain such as the thalamus and superior frontal, which were previously associated with information integration and communication between brain areas (Bell & Shine, 2016; Gong et al., 2009; Hagmann et al., 2008; Oldham & Fornito, 2019; van den Heuvel & Sporns, 2011; van den Heuvel & Sporns, 2013; Zamora-López et al., 2010; Zamora-López et al., 2011).

The representation of integrated and segregated states with modularity and global efficiency creates a continuum rather than two separated communities as it can be seen in Figure 2, where high modularity is represented by low global efficiency and vice versa. This can be expected as brain activity is represented by oxygenated blood flow in fMRI that continuously fluctuates in this study. The k-means clustering, used in this study to separate the two states, poses some separation limitations, especially in the case of a continual axis; however, our results that showed differences between the two states indicated that the points on the extreme ends drive the underlying manifold even in the case of a superficial partition of the states. Further analysis can employ different techniques either in a regression manner or focused specifically on the points leaning towards the high ends of the spectra.

The 2D representation of the latent space was purposefully chosen for easier interpretability and visualization. Multidimensional representations might capture the underlying brain dynamics more appropriately; however, they are limitations in visualizations and their explanations. In the 2D space, some of the finer differences might be diminished as the space accounts only for two features, but the important space occupancy difference is preserved.

Our results suggest, that in the time of our dataset (yet limited by just 175 time points), segregated states are more common during all of the scanning sessions. This also results from the decision to have

only two states without the middle transition or balance state. From previous studies, we can infer that the middle state would lead in occupancy probability (Wang et al., 2021). From previous studies (Engel et al., 2013; Galindo-Leon et al., 2019; Guggisberg et al., 2015; Krienen et al., 2014), there is an evidence that integration has at least two forms in rest. The first one is interhemispheric alignment of beta amplitudes and intrahemispheric phase-locking in alpha rhythms. Previous results also showed that integration states predominantly visit the default mode, frontoparietal control, salience, and dorsal and ventral attention networks (Margulies et al., 2016; Vatansever et al., 2015) and that functional modules are temporally flexible upon modulation through early learning (Bassett et al., 2011). From our results, the most functionally connected brain areas in the integration states are known to be members of the default mode network such as superior frontal lobules, inferior parietal lobules and a gateway to the default mode network thalamus (Liao et al., 2010; Zhou et al., 2020). However, the latent space features represent the whole connectivity matrices without the possibility of examining specific RSNs, which poses a limitation of the study. Further investigation into the switching of RSNs in integration and segregation could bring more clarification into our cognitive understanding.

We identified important fluctuations between global efficiency / local efficiency and high modularity / low modularity in working memory tasks; this is probably due to the design of the task where there are parts requiring high cognitive load, and parts of rest/low cognitive load indicating the necessity of fast switching and flexibility between cognitively demanding assignments and rest. Similar switching was also demonstrated in social and language tasks. Rest, along with gambling and emotion tasks, generated less switching and a steadier tendency, showing general lower switching between cognitive loads and rest periods.

After training the autoencoder, extraction of its 2D latent space revealed that the occupation of the manifold is significantly more compact in the integrated state than in the segregated one. The integrated state was represented in fewer time points than the segregated state, so we tested whether the compactness could be due to a lower number of data points. After balancing the dataset to validate the autoencoder, similar results were obtained. We also trained the autoencoder more times, and similarly the results showed less space occupation in the integrated state.

From our classification results, we can conclude that modularity and global efficiency are good metrics for modalities' separation. Both states scored high accuracy; however, better results were in the integrated state, which we predicted to have a lower score. This can be due to the data specificity as the segregated state has more data points, which can also be much noisier. The next approach could include three states, where all the middle undecided data points would belong to a special state and not in the segregated one. Some future investigation can also include a dynamical approach (Gilson et al., 2018; Gilson et al., 2019) to graph analysis and gain more insight into how spatio-temporal information flows shape segregation and integration in the brain.

5 | CONCLUSION

We have clustered two states in brain dynamics: integrated and segregated. We have shown that the integrated state occupies less space on an underlying manifold and is represented with lower entropy compared with the segregated state. With this finding, we proved that integration is characterised by data compression while segregation is represented with divergency. We have demonstrated that the brain activity in resting-state exhibits larger entropy as compared with tasks due to a more random wandering between states. Also, that for the segregated states the difference in entropy is significant between rest and the tasks, pointing towards the specificity in tasks during segregation.

AUTHOR CONTRIBUTIONS

Katerina Capouskova: Conceptualisation, methodology, software, validation, formal analysis, investigation, data curation, writing—original draft, visualisation. Gorka Zamora-López: Conceptualisation, methodology, writing—review and editing, supervision, funding acquisition. Morten L. Kringelbach: Data curation, writing—review and editing, supervision, visualisation. Gustavo Deco: Conceptualisation, methodology, formal analysis, resources, writing—review and editing, supervision, project administration, funding acquisition.

ACKNOWLEDGEMENTS

K. C, G. Z.-L., and G. D. are supported by the HBP SGA3 Human Brain Project Specific Grant Agreement 3 (grant agreement no. 945539), funded by the EU H2020 FET Flagship Programme; G. D. is supported by Project PID2022-136216NB-I00 financed by the MCIN / AEI/ 1013039 / 501100011033 / FEDER, UE., the Ministry of Science and Innovation, the State Research Agency and the European Regional Developmental Fund, and by AGAUR research support grant (ref. 2021 SGR 00917) funded by the Department of Research and Universities of the Generalitat of Catalunya. M. L. K. is supported by the ERC Consolidator Grant: CAREGIVING (No. 615539), Center for Music in the Brain, funded by the Danish National Research Foundation (DNRF117), and Centre for Eudaimonia and Human Flourishing funded by the Pettit and Carlsberg Foundations. The funding bodies had neither influence in the research design, data collection, and analysis nor will in preparing and publishing the manuscript.

CONFLICT OF INTEREST STATEMENT

The authors declare no competing financial interests.

DATA AVAILABILITY STATEMENT

The data that support the findings of this study are openly available in Human Connectome Project at https://www.humanconnectome.org/study/hcp-young-adult/data-releases.

ORCID

Katerina Capouskova https://orcid.org/0000-0002-1247-943X
Morten L. Kringelbach https://orcid.org/0000-0002-3908-6898

REFERENCES

Agarap, A. F. (2018). Deep learning using rectified linear units (ReLU). Retrieved from https://arxiv.org/abs/1803.08375v2

Altan, E., Solla, S. A., Miller, L. E., & Perreault, E. J. (2021). Estimating the dimensionality of the manifold underlying multi-electrode neural recordings. *PLoS Computational Biology*, *17*, e1008591.

Baars, B. J. (2009). *In the theater of consciousness: The workspace of the mind*. Oxford Academic Books.

Barch, D. M., Burgess, G. C., Harms, M. P., Petersen, S. E., Schlaggar, B. L., Corbetta, M., Glasser, M. F., Curtiss, S., Dixit, S., Feldt, C., Nolan, D., Bryant, E., Hartley, T., Footer, O., Bjork, J. M., Poldrack, R., Smith, S., Johansen-Berg, H., Snyder, A. Z., & Van Essen, D. C. (2013). Function in the human connectome: Task-fMRI and individual differences in behavior. *NeuroImage*, *80*, 169–189.

Bassett, D. S., Wymbs, N. F., Porter, M. A., Mucha, P. J., Carlson, J. M., & Grafton, S. T. (2011). Dynamic reconfiguration of human brain networks during learning. *Proceedings of the National Academy of Sciences of the United States of America*, *108*, 7641–7646.

Bell, P. T., & Shine, J. M. (2016). Subcortical contributions to large-scale network communication. *Neuroscience and Biobehavioral Reviews*, *71*, 313–322.

Betzel, R. F., Fukushima, M., He, Y., Zuo, X. N., & Sporns, O. (2016). Dynamic fluctuations coincide with periods of high and low modularity in resting-state functional brain networks. *NeuroImage*, *127*, 287–297. Retrieved from https://pubmed.ncbi.nlm.nih.gov/26687667/

Blondel, V. D., Guillaume, J. L., Lambiotte, R., & Lefebvre, E. (2008). Fast unfolding of communities in large networks. *Journal of Statistical Mechanics: Theory and Experiment*, *2008*, P10008. https://doi.org/10.1088/1742-5468/2008/10/P10008

Bouyssi-Kobar, M., De Asis-Cruz, J., Murnick, J., Chang, T., & Limperopoulos, C. (2019). Altered functional brain network integration, segregation, and modularity in infants born very preterm at term-equivalent age. *The Journal of Pediatrics*, *213*, 13–21.e1.

Bressler, S. L., & Kelso, J. A. S. (2001). Cortical coordination dynamics and cognition. *Trends in Cognitive Sciences*, *5*, 26–36.

Cabral, J., Vidaurre, D., Marques, P., Magalhães, R., Silva Moreira, P., Miguel Soares, J., Deco, G., Sousa, N., & Kringelbach, M. L. (2017). Cognitive performance in healthy older adults relates to spontaneous switching between states of functional connectivity during rest. *Scientific Reports*, *7*, 5135.

Capouskova, K., Kringelbach, M. L., & Deco, G. (2022). Modes of cognition: Evidence from metastable brain dynamics. *NeuroImage*, *260*, 119489.

Carhart-Harris, R. L., Leech, R., Hellyer, P. J., Shanahan, M., Feilding, A., Tagliazucchi, E., Chialvo, D. R., & Nutt, D. (2014). The entropic brain: A theory of conscious states informed by neuroimaging research with psychedelic drugs. *Frontiers in Human Neuroscience*, *8*, 20. https://doi.org/10.3389/fnhum.2014.00020/abstract

Casanova, R., Lyday, R. G., Bahrami, M., Burdette, J. H., Simpson, S. L., & Laurienti, P. J. (2021). Embedding functional brain networks in low dimensional spaces using manifold learning techniques. *Frontiers in Neuroinformatics*, *15*, 740143.

Chaudhuri, R., Gerçek, B., Pandey, B., Peyrache, A., & Fiete, I. (2019). The intrinsic attractor manifold and population dynamics of a canonical cognitive circuit across waking and sleep. *Nature Neuroscience*, *22*, 1512–1520.

Cocuzza, C. V., Ito, T., Schultz, D., Bassett, D. S., & Cole, M. W. (2020). Flexible coordinator and switcher hubs for adaptive task control. *The Journal of Neuroscience*, *40*, 6949–6968.

Cohen, J. R., & D'Esposito, M. (2016). The segregation and integration of distinct brain networks and their relationship to cognition. *The Journal of Neuroscience*, *36*, 12083–12094.

Cole, M. W., Reynolds, J. R., Power, J. D., Repovs, G., Anticevic, A., & Braver, T. S. (2013). Multi-task connectivity reveals flexible hubs for adaptive task control. *Nature Neuroscience*, *169*(16), 1348–1355.

Damasio, A. R. (1989). The brain binds entities and events by multiregional activation from convergence zones. *Neural Computation*, *1*, 123–132.

Deco, G., Cabral, J., Woolrich, M. W., Stevner, A. B. A., van Hartevelt, T. J., & Kringelbach, M. L. (2017). Single or multiple frequency generators in on-going brain activity: A mechanistic whole-brain model of empirical MEG data. *NeuroImage*, *152*, 538–550.

Deco, G., & Kringelbach, M. (2016). Metastability and coherence: Extending the communication through coherence hypothesis using a whole-brain computational perspective. *Trends in Neurosciences*, *39*, 432

Deco, G., Tononi, G., Boly, M., & Kringelbach, M. L. (2015). Rethinking segregation and integration: Contributions of whole-brain modelling. *Nature Reviews. Neuroscience*, *16*, 430–439.

Dehaene, S., & Changeux, J. P. (2011). Experimental and theoretical approaches to conscious processing. *Neuron*, *70*, 200–227.

Demirtaş, M., Ponce-Alvarez, A., Gilson, M., Hagmann, P., Mantini, D., Betti, V., Romani, G. L., Friston, K., Corbetta, M., & Deco, G. (2019). Distinct modes of functional connectivity induced by movie-watching. *NeuroImage*, *184*, 335–348.

Desikan, R. S., Ségonne, F., Fischl, B., Quinn, B. T., Dickerson, B. C., Blacker, D., Buckner, R. L., Dale, A. M., Maguire, R. P., Hyman, B. T., Albert, M. S., & Killiany, R. J. (2006). An automated labeling system for subdividing the human cerebral cortex on MRI scans into gyral based regions of interest. *NeuroImage*, *31*, 968–980.

Engel, A. K., Gerloff, C., Hilgetag, C. C., & Nolte, G. (2013). Intrinsic coupling modes: Multiscale interactions in ongoing brain activity. *Neuron*, *80*(4), 867–886.

Escrichs, A., Sanjuán, A., Atasoy, S., López-González, A., Garrido, C., Càmara, E., & Deco, G. (2019). Characterizing the dynamical complexity underlying meditation. *Frontiers in Systems Neuroscience*, *13*, 27. https://doi.org/10.3389/fnsys.2019.00027/full

Fong, A. H. C., Yoo, K., Rosenberg, M. D., Zhang, S., Li, C.-S. R., Scheinost, D., Constable, R. T., & Chun, M. M. (2019). Dynamic functional connectivity during task performance and rest predicts individual differences in attention across studies. *NeuroImage*, *188*, 14–25.

Galindo-Leon, E. E., Stitt, I., Pieper, F., Stieglitz, T., Engler, G., & Engel, A. K. (2019). Context-specific modulation of intrinsic coupling modes shapes multisensory processing. *Science Advances*, *5*, eaar7633.

Gallego, J. A., Perich, M. G., Miller, L. E., & Solla, S. A. (2017). Neural manifolds for the control of movement. *Neuron*, *94*, 978–984.

Gao, P., & Ganguli, S. (2015). On simplicity and complexity in the brave new world of large-scale neuroscience. *Current Opinion in Neurobiology*, *32*, 148–155.

Gao, S., Mishne, G., & Scheinost, D. (2021). Nonlinear manifold learning in functional magnetic resonance imaging uncovers a low-dimensional space of brain dynamics. *Human Brain Mapping*, *42*, 4510–4524.

Gilson, M., Kouvaris, N. E., Deco, G., Mangin, J.-F., Poupon, C., Lefranc, S., Rivière, D., & Zamora-López, G. (2019). Network analysis of whole-brain fMRI dynamics: A new framework based on dynamic communicability. *NeuroImage*, *201*, 116007.

Gilson, M., Kouvaris, N. E., Deco, G., & Zamora-López, G. (2018). Framework based on communicability and flow to analyze complex network dynamics. *Physical Review E*, *97*, 052301. https://doi.org/10.1103/PhysRevE.97.052301

Glasser, M. F., Coalson, T. S., Robinson, E. C., Hacker, C. D., Harwell, J., Yacoub, E., Ugurbil, K., Andersson, J., Beckmann, C. F., Jenkinson, M., Smith, S. M., & Van Essen, D. C. (2016). A multi-modal parcellation of human cerebral cortex. *Nature*, *536*, 171–178.

Glasser, M. F., Sotiropoulos, S. N., Wilson, J. A., Coalson, T. S., Fischl, B., Andersson, J. L., Xu, J., Jbabdi, S., Webster, M., Polimeni, J. R., Van Essen, D. C., & Jenkinson, M. (2013). The minimal preprocessing pipelines for the human connectome project. *NeuroImage*, *80*, 105–124.

Gong, G., He, Y., Concha, L., Lebel, C., Gross, D. W., Evans, A. C., & Beaulieu, C. (2009). Mapping anatomical connectivity patterns of human cerebral cortex using in vivo diffusion tensor imaging

tractography. *Cerebral Cortex*, *19*, 524–536. https://doi.org/10.1093/cercor/bhn102

Griffanti, L., Salimi-Khorshidi, G., Beckmann, C. F., Auerbach, E. J., Douaud, G., Sexton, C. E., Zsoldos, E., Ebmeier, K. P., Filippini, N., Mackay, C. E., Moeller, S., Xu, J., Yacoub, E., Baselli, G., Ugurbil, K., Miller, K. L., & Smith, S. M. (2014). ICA-based artefact removal and accelerated fMRI acquisition for improved resting state network imaging. *NeuroImage*, *95*, 232–247.

Guggisberg, A. G., Rizk, S., Ptak, R., Di Pietro, M., Saj, A., Lazeyras, F., Lovblad, K. O., Schnider, A., & Pignat, J. M. (2015). Two intrinsic coupling types for resting-state integration in the human brain. *Brain Topography*, *28*(2), 318–329.

Hagmann, P., Cammoun, L., Gigandet, X., Meuli, R., Honey, C. J., Wedeen, V. J., & Sporns, O. (2008). Mapping the structural core of human cerebral cortex. *PLoS Biology*, *6*, e159. https://doi.org/10.1371/journal.pbio.0060159

He, L., Zhuang, K., Li, Y., Sun, J., Meng, J., Zhu, W., Mao, Y., Chen, Q., Chen, X., & Qiu, J. (2019). Brain flexibility associated with need for cognition contributes to creative achievement. *Psychophysiology*, *56*, e13464. https://doi.org/10.1111/psyp.13464

Hilgetag, C. C., & Kaiser, M. (2004). Clustered organization of cortical connectivity. *Neuroinformatics*, *2*, 353–360.

Hinton, G. E., & Salakhutdinov, R. R. (2006). Reducing the dimensionality of data with neural networks. *Science*, *313*(80), 504 LP–507.

Ito, T., & Murray, J. D. (2021). Multi-task representations in human cortex transform along a sensory-to-motor hierarchy. bioRxiv.

Kaufman, L., & Rousseeuw, P. J. (2005). In L. Kaufman & P. J. Rousseeuw (Eds.), *Finding groups in data*. John Wiley & Sons. https://doi.org/10.1002/9780470316801

Keerativittayayut, R., Aoki, R., Sarabi, M. T., Jimura, K., & Nakahara, K. (2018). Large-scale network integration in the human brain tracks temporal fluctuations in memory encoding performance. *eLife*, *7*, e32696.

Kingma, D. P., & Ba, J. (2014). Adam: A method for stochastic optimization. Retrieved from http://arxiv.org/abs/1412.6980

Klein, A., & Tourville, J. (2012). 101 labeled brain images and a consistent human cortical labeling protocol. *Frontiers in Neuroscience*, *6*, 171. https://doi.org/10.3389/fnins.2012.00171/abstract

Krienen, F. M., Thomas Yeo, B. T., & Buckner, R. L. (2014). Reconfigurable task-dependent functional coupling modes cluster around a core functional architecture. *Philosophical Transactions of the Royal Society B*, *369*, 20130526.

Kumar, K., Toews, M., Chauvin, L., Colliot, O., & Desrosiers, C. (2018). Multi-modal brain fingerprinting: A manifold approximation based framework. *NeuroImage*, *183*, 212–226.

Latora, V., & Marchiori, M. (2001). Efficient behavior of small-world networks. *Physical Review Letters*, *87*, 198701. https://doi.org/10.1103/PhysRevLett.87.198701

Latora, V., & Marchiori, M. (2003). Economic small-world behavior in weighted networks. *European Physical Journal B: Condensed Matter and Complex Systems*, *322*(32), 249–263. https://doi.org/10.1140/epjb/e2003-00095-5

Lemaître, G., Nogueira, F., & Aridas, C. K. (2017). Imbalanced-learn: A Python toolbox to tackle the curse of imbalanced datasets in machine learning. *Journal of Machine Learning Research*, *18*, 1–5.

Liao, W., Zhang, Z., Pan, Z., Mantini, D., Ding, J., Duan, X., Luo, C., Lu, G., & Chen, H. (2010). Altered functional connectivity and small-world in mesial temporal lobe epilepsy. *PLoS One*, *5*, e8525.

Margulies, D. S., Ghosh, S. S., Goulas, A., Falkiewicz, M., Huntenburg, J. M., Langs, G., Bezgin, G., Eickhoff, S. B., Castellanos, F. X., Petrides, M., Jefferies, E., & Smallwood, J. (2016). Situating the default-mode network along a principal gradient of macroscale cortical organization. *Proceedings of the National Academy of Sciences of the United States of America*, *113*, 12574–12579.

McInnes, L., Healy, J., Saul, N., & Großberger, L. (2018). UMAP: Uniform manifold approximation and projection. *Journal of Open Source Software*, *3*, 861.

Mohr, H., Wolfensteller, U., Betzel, R. F., Mišić, B., Sporns, O., & Richiardi, J. (2016). Integration and segregation of large-scale brain networks during short-term task automatization. *Nature Communications*, *71*(7), 1–12.

Navarro Schröder, T., Haak, K. V., Zaragoza Jimenez, N. I., Beckmann, C. F., & Doeller, C. F. (2015). Functional topography of the human entorhinal cortex. *eLife*, *4*, e06738.

Newman, M. E. J. (2004). Fast algorithm for detecting community structure in networks. *Physical Review E*, *69*.

Nogueira, R., Lawrie, S., & Moreno-Bote, R. (2018). Neuronal variability as a proxy for network state. *Trends in Neurosciences*, *41*, 170–173.

Oldham, S., & Fornito, A. (2019). The development of brain network hubs. *Developmental Cognitive Neuroscience*, *36*, 100607.

Oostenveld, R., Fries, P., Maris, E., & Schoffelen, J.-M. (2011). FieldTrip: Open source software for advanced analysis of MEG, EEG, and invasive electrophysiological data. *Computational Intelligence and Neuroscience*, *2011*, 1–9.

Pedregosa, F., Varoquaux, G., Gramfort, A., Michel, V., Thirion, B., Grisel, O., Blondel, M., Prettenhofer, P., Weiss, R., Dubourg, V., Vanderplas, J., Passos, A., Cournapeau, D., Brucher, M., Perrot, M., & Duchesnay, É. (2011). Scikit-learn: Machine learning in Python. *Journal of Machine Learning Research*, *12*, 2825–2830.

Plassard, A. J., Davis, L. T., Newton, A. T., Resnick, S. M., Landman, B. A., & Bermudez, C. (2018). Learning implicit brain MRI manifolds with deep learning. *Proceedings of SPIE – The International Society for Optical Engineering*, *10574*, 105741L.

Ponce-Alvarez, A., Deco, G., Hagmann, P., Romani, G. L., Mantini, D., & Corbetta, M. (2015). Resting-state temporal synchronization networks emerge from connectivity topology and heterogeneity. *PLoS Computational Biology*, *11*, e1004100. https://doi.org/10.1371/journal.pcbi.1004100

Power, J. D., Cohen, A. L., Nelson, S. M., Wig, G. S., Barnes, K. A., Church, J. A., Vogel, A. C., Laumann, T. O., Miezin, F. M., Schlaggar, B. L., & Petersen, S. E. (2011). Functional network organization of the human brain. *Neuron*, *72*, 665–678.

Reichardt, J., & Bornholdt, S. (2006). *Statistical mechanics of community detection*. Physical Review E.

Ren, S., Li, J., Taya, F., DeSouza, J., Thakor, N. V., & Bezerianos, A. (2017). Dynamic functional segregation and integration in human brain network during complex tasks. *IEEE Transactions on Neural Systems and Rehabilitation Engineering*, *25*, 547–556.

Ronan, T., Qi, Z., & Naegle, K. M. (2016). Avoiding common pitfalls when clustering biological data. *Science Signaling*, *9*, re6.

Rousseeuw, P. J. (1987). Silhouettes: A graphical aid to the interpretation and validation of cluster analysis. *Journal of Computational and Applied Mathematics*, *20*, 53–65.

Rué-Queralt, J., Stevner, A., Tagliazucchi, E., Laufs, H., Kringelbach, M. L., Deco, G., & Atasoy, S. (2021). Decoding brain states on the intrinsic manifold of human brain dynamics across wakefulness and sleep. *Communications Biology*, *4*, 854.

Saenger, V. M., Ponce-Alvarez, A., Adhikari, M., Hagmann, P., Deco, G., & Corbetta, M. (2018). Linking entropy at rest with the underlying structural connectivity in the healthy and lesioned brain. *Cerebral Cortex*, *28*, 2948 –2958.

Salimi-Khorshidi, G., Douaud, G., Beckmann, C. F., Glasser, M. F., Griffanti, L., & Smith, S. M. (2014). Automatic denoising of functional MRI data: Combining independent component analysis and hierarchical fusion of classifiers. *NeuroImage*, *90*, 449–468.

Scannell, J. W., Blakemore, C., & Young, M. P. (1995). Analysis of connectivity in the cat cerebral cortex. *The Journal of Neuroscience*, *15*, 1463–1483.

Scannell, J. W., & Young, M. P. (1993). The connectional organization of neural systems in the cat cerebral cortex. *Current Biology*, *3*, 191–200.

Senden, M., Reuter, N., van den Heuvel, M. P., Goebel, R., & Deco, G. (2017). Cortical rich club regions can organize state-dependent functional network formation by engaging in oscillatory behavior. *NeuroImage*, *146*, 561–574.

Senden, M., Reuter, N., van den Heuvel, M. P., Goebel, R., Deco, G., & Gilson, M. (2018). Task-related effective connectivity reveals that the cortical rich club gates cortex-wide communication. *Human Brain Mapping*, *39*, 1246–1262. https://doi.org/10.1002/hbm.23913

Shanahan, M., Bingman, V. P., Shimizu, T., Wild, M., & Güntürkün, O. (2013). Large-scale network organisation in the avian forebrain: A connectivity matrix and theoretical analysis. *Frontiers in Computational Neuroscience* *7*, 89.

Shine, J. M., Breakspear, M., Bell, P. T., Ehgoetz Martens, K. A., Shine, R., Koyejo, O., Sporns, O., & Poldrack, R. A. (2019). Human cognition involves the dynamic integration of neural activity and neuromodulatory systems. *Nature Neuroscience*, *22*, 289–296.

Smith, S. M., Beckmann, C. F., Andersson, J., Auerbach, E. J., Bijsterbosch, J., Douaud, G., Duff, E., Feinberg, D. A., Griffanti, L., Harms, M. P., Kelly, M., Laumann, T., Miller, K. L., Moeller, S., Petersen, S., Power, J., Salimi-Khorshidi, G., Snyder, A. Z., Vu, A. T., … Glasser, M. F. (2013). Resting-state fMRI in the human connectome project. *NeuroImage*, *80*, 144–168.

Tononi, G. (2004). An information integration theory of consciousness. *BMC Neuroscience*, *5*, 42.

van den Heuvel, M. P., & Sporns, O. (2011). Rich-club organization of the human connectome. *The Journal of Neuroscience*, *31*, 15775–15786.

van den Heuvel, M. P., & Sporns, O. (2013). Network hubs in the human brain. *Trends in Cognitive Sciences*, *17*, 683–696.

Vatansever, D., Menon, D. K., Manktelow, A. E., Sahakian, B. J., & Stamatakis, E. A. (2015). Default mode dynamics for global functional integration. *The Journal of Neuroscience*, *35*, 15254–15262.

Vila-Vidal, M., Capouskova, K., Atasoy, S., Kringelbach, M. L., & Deco, G. (2019). Uncovering the spatiotemporal scales of common neuromental constructs: Comment on "Is temporo-spatial dynamics the 'common currency' of brain and mind? In quest of 'Spatiotemporal Neuroscience'" by Georg Northoff et al. *Physics of Life Reviews*, *33*, 64–66.

Virtanen, P., Gommers, R., Oliphant, T. E., Haberland, M., Reddy, T., Cournapeau, D., Burovski, E., Peterson, P., Weckesser, W., Bright, J., van der Walt, S. J., Brett, M., Wilson, J., Millman, K. J., Mayorov, N., Nelson, A. R. J., Jones, E., Kern, R., Larson, E., … Vázquez-Baeza, Y. (2020). SciPy 1.0: Fundamental algorithms for scientific computing in Python. *Nature Methods*, *173*(17), 261–272.

Vohryzek, J., Deco, G., Cessac, B., Kringelbach, M. L., & Cabral, J. (2020). Ghost attractors in spontaneous brain activity: Recurrent excursions into functionally-relevant BOLD phase-locking states. *Frontiers in Systems Neuroscience*, *14*, 20. https://doi.org/10.3389/fnsys.2020.00020/full

Wang, R., Liu, M., Cheng, X., Wu, Y., Hildebrandt, A., & Zhou, C. (2021). Segregation, integration, and balance of large-scale resting brain networks configure different cognitive abilities. *Proceedings of the National Academy of Sciences of the United States of America*, *118*, e2022288118.

Williams, A. H., Kim, T. H., Wang, F., Vyas, S., Ryu, S. I., Shenoy, K. V., Schnitzer, M., Kolda, T. G., & Ganguli, S. (2018). Unsupervised discovery of Demixed, low-dimensional neural dynamics across multiple timescales through tensor component analysis. *Neuron*, *98*, 1099–1115.e8.

Yang, G. R., Cole, M. W., & Rajan, K. (2019). How to study the neural mechanisms of multiple tasks. *Current Opinion in Behavioral Sciences*, *29*, 134–143.

Zamora-López, G., Zhou, C., & Kurths, J. (2010). Cortical hubs form a module for multisensory integration on top of the hierarchy of cortical networks. *Frontiers in Neuroinformatics*, *4*, 1.

Zamora-López, G., Zhou, C., & Kurths, J. (2011). Exploring brain function from anatomical connectivity. *Frontiers in Neuroscience*, *5*, 83. https://doi.org/10.3389/fnins.2011.00083/abstract

Zhou, H. X., Chen, X., Shen, Y. Q., Li, L., Chen, N. X., Zhu, Z. C., Castellanos, F. X., & Yan, C. G. (2020). Rumination and the default mode network: Meta-analysis of brain imaging studies and implications for depression. *NeuroImage*, *206*, 116287.

Zhuang, F., Cheng, X., Luo, P., Pan, S. J., & He, Q. (2017). Supervised representation learning with double encoding-layer autoencoder for transfer learning. *ACM Transactions on Intelligent Systems and Technology*, *9*, 1–17.

SUPPORTING INFORMATION

Additional supporting information can be found online in the Supporting Information section at the end of this article.

How to cite this article: Capouskova, K., Zamora-López, G., Kringelbach, M. L., & Deco, G. (2023). Integration and segregation manifolds in the brain ensure cognitive flexibility during tasks and rest. *Human Brain Mapping*, *44*(18), 6349–6363. https://doi.org/10.1002/hbm.26511